Structure-Directing and Template Roles of Aromatic Molecules in the Self-Assembly Formation Process of 3D Holmium–Succinate MOFs

María C. Bernini,[†,‡] Natalia Snejko,[†] Enrique Gutierrez-Puebla,[†] Elena V. Brusau,[‡] Griselda E. Narda,[‡] and M. Ángeles Monge*,[†]

[†]Instituto de Ciencia de Materiales de Madrid, CSIC, Madrid, Spain

[‡]Área de Química General e Inorgánica "Dr. G. F. Puelles", Facultad de Química, Bioquímica y Farmacia, Universidad Nacional de San Luis, Chacabuco y Pedernera, 5700 San Luis, Argentina

S *Supporting Information*

ABSTRACT: Two new holmium–succinate frameworks have been synthesized by hydrolysis in situ of the succinylsalicylic acid under different hydrothermal conditions. Compound **1**, $[Ho_2(C_4H_4O_4)_3(H_2O)_2] \cdot 0.33(C_7H_6O_3)$, $P\bar{1}$ space group, has a novel structure composed by 1D-SBUs consisting of $[HoO_9]$ chains of polyhedra linked by the succinate ligands giving a 3D framework. Compound **2**, $[Ho_2(C_4H_4O_4)_3(H_2O)_2]$, also belonging to the $P\bar{1}$ space group, has a denser structure. The role of the in-situ-generated salicylic acid on formation of both structures is studied by means of a synthesis design methodology. A topological study of the new holmium succinate compounds in comparison with the previously reported 3D holmium–succinate framework is performed here.
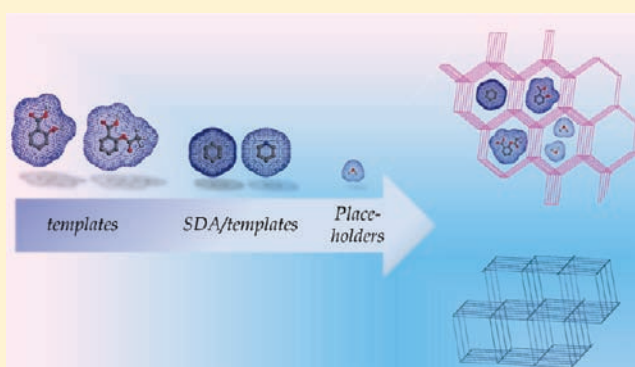
INTRODUCTION

Nanospaced metal organic frameworks (MOFs) usually have unique characteristics: regular nanosized pores, flexibility, and a designed pore surface that can have diverse functionalities, such as gas storage,[1] separation,[2] catalysis,[3] drug release/delivery,[4] embedding of metal nanoparticles for applications in catalysis and sensor technology,[5] etc.

It is well known that during the self-assembly process, structure-directing agents or templates are crucial for the synthesis of 3D porous structures and are most successfully used in the synthesis of zeolites in order to obtain novel open frameworks.[6] However, the use of templates in MOFs materials remains relatively less explored; thus, the distinction between a structure-directing agent (SDA) and a true template is perhaps rather subtle in this subject. Recently, a template has been defined as "an agent that favors formation of a specific open framework under a broad range of conditions and that accelerates the crystallization".[7]

The succinate-based MOFs systems have been widely studied; several structures have been reported using not only transition metal (TM)[8] ions but also rare earth (REE) ones.[9] In relation with TM ions, topological control is rendered by taking advantage of their predictable coordination geometries. However, the REE ions that exhibit high coordination numbers and diversity of possible coordination polyhedra are considered a major challenge in order to generate open MOFs with a certain structure.

Continuing with our previous studies in REE succinates,[10−12] employing different aromatic molecules as SDAs or templates in order to obtain different holmium–succinate MOFs is addressed here.

It is a known fact that in superheated solution conditions, some changes in the ligand molecule itself can occur.[13] Examples exist when ligand functional groups are added,[14] removed,[15] or changed[16] and when ligand molecules are cleaved[17] or condensed with other molecules that are present in the reaction medium.[18]

In our case, two new Ho(III) compounds have been synthesized by hydrolysis in situ of the succinylsalicylic acid under different hydrothermal conditions. The role of the in-situ-generated salicylic acid on formation of both structures is explored by a synthesis design methodology. A topological study of the corresponding frameworks in comparison with previously synthesized REE 3D MOFs is given here. A complete characterization of compound **1** by X-ray diffraction, spectroscopic, and thermal techniques is reported.

EXPERIMENTAL SECTION

Synthesis. The compound $[Ho_2(C_4H_4O_4)_3(H_2O)_2] \cdot 0.33(C_7H_6O_3)$ (**1**) was obtained by hydrothermal reaction of 0.5 mmol of $Ho(NO_3)_3 \cdot 5H_2O$

Table 1. Crystal Data and Structure Refinement for 1 and 2

	1	2
empirical formula	$C_{12} H_{12} Ho_2 O_{14}$[a]	$C_{12} H_{12} Ho_2 O_{14}$
fw	710.08	710.08
temperature	room temperature	173 (2) K
wavelength	0.71073 Å	0.71073 Å
cryst syst	triclinic	triclinic
space group	$P\bar{1}$	$P\bar{1}$
unit cell dimensions	a = 7.6112(18) Å	a = 7.5940(15) Å
	b = 11.927(3) Å	b = 8.4230(17) Å
	c = 12.130(3) Å	c = 13.829(3) Å
	α = 67.602(4)°	α = 96.64(3)°
	β = 89.920(4)°	β = 98.38(3)°
	γ = 80.498(4)°	γ = 99.03(3)°
volume	1001.8(4) Å³	855.5(3) Å³
Z	2	2
density (calcd)	2.354 Mg/m³	2.756 Mg/m³
abs coeff	7.906 mm⁻¹	9.257 mm⁻¹
F(000)	660	660
cryst size	0.10 × 0.04 × 0.04 mm³	0.20 × 0.12 × 0.10 mm³
theta range for data collection	1.82−28.35°	1.50−28.96°
index ranges	(−10, 9), (−15,15), (−15,15)	(−10,10), (−10,11), (−18,18)
reflns collected	7472	6869
independent reflns	4046 [R(int) = 0.0826]	3744 [R(int) = 0.0844]
abs corr	semiempirical	semiempirical
refinement method	full-matrix least-squares on F^2	full-matrix least-squares on F^2
data/restraints/parameters	4046/0/123	3744/0/244
goodness-of-fit on F^2	0.934	0.926
final R indices $[I > 2\sigma(I)]$	R1 = 0.0723, wR2 = 0.1720	R1 = 0.0578, wR2 = 0.0965
R indices (all data)	R1 = 0.1309, wR2 = 0.1937	R1 = 0.1211, wR2 = 0.1138
largest diff. peak and hole	3.544 and −3.762 e·Å⁻³	3.695 and −2.376 e·Å⁻³

[a] The reported formula does not account for the channels content in 1.

with 0.75 mmol of succinylsalicylic acid ($H_2C_{18}H_{12}O_8$) in 10 mL of distilled water, adjusting the pH to 5.5 with 0.2 mL of triethylamine (TEA). The mixture was placed in a Teflon-lined digestion bomb of 43 mL internal volume, heated for 65 h at 160 °C, and then cooled to room temperature. Small crystals were obtained as light brown needles, which were separated by filtration, washed with distilled water and acetone, and dried at ambient conditions.

Pure compound **1** as a microcrystalline powder was obtained by heating the same reaction mixture for 1 h at 105 °C. The purity of this sample was verified by elemental analysis and PXRD patterns (see Supporting Information, Figure S1-a). These experimental conditions are denoted from now on as A-methodology.

When the same initial mixture of reagents is heated for 65 h at 180−200 °C, a minor phase with formula $[Ho_2(C_4H_4O_4)_3(H_2O)_2]$ (**2**) is obtained as prismatic brown single crystals along with a crystalline powder of a third unidentified compound.

On the other hand, compound **1** can also be synthesized by hydrothermal reaction of 0.5 mmol of $Ho(NO_3)_3 \cdot 5H_2O$ with 0.75 mmol of succinic acid ($C_4H_6O_4$) in the presence of 5 mmol of salicylic acid in 10 mL of distilled water, adjusting the pH to 5.5 with 0.2 mL of TEA. The mixture is placed in a Teflon-lined digestion bomb during 96 h at 160 °C and then cooled to room temperature; light brown needle-shaped crystals are obtained. These experimental conditions are denoted from now on as B-methodology. The purity of this sample was confirmed by elemental analysis and PDRX patterns (see Supporting Information, Figure S1-b).

Crystal Structure Determination. Table 1 summarizes the main crystal and refinement data for the new compounds. Crystals were selected under a polarizing optical microscope and glued on a glass fiber for a single-crystal X-ray diffraction (XRD) experiment. X-ray intensity data were collected in a Bruker SMART CCD diffractometer which is equipped with a normal focus, 2.4 kW sealed tube X-ray source (Mo Kα radiation = 0.71073 Å). Data were collected at room temperature and at 173 K for compounds **1** and **2**, respectively, over a hemisphere of the reciprocal space by a combination of three sets of exposures. Each exposure of 10 s covered 0.3° in ω. Unit cell dimensions were determined by a least-squares fit of reflections with $I > 2 \sigma(I)$. Data were integrated and scaled using the SAINTplus program.[19] A semiempirical absorption and scale correction based on equivalent reflection was carried out using SADABS.[20] Space group determinations were carried out using XPREP.[21] The structures were solved by direct methods. Several attempts were made to get better data (quite a few crystals and temperature measurements and absorption corrections), but the obtained data completeness for both compounds was still low, and consequently both refinements had some troubles.

In the case of compound **1**, besides the small crystal size, low crystallinity, and crystals being frequently twinned, once the structure was solved, a continuous electron density was observed all along the main channels. After trying several disorder models involving aromatic molecules, we gave up and extracted the electron density with the Platon squeeze program. The removed electron density of ~45 e⁻ per unit cell agrees with the chemically determined $[Ho_2(C_4H_4O_4)_3(H_2O)_2]\cdot0.33\text{-}(C_7H_6O_3)$ formula, and Z = 2 (48 e⁻).

Compound **2** crystals did not diffract at high angles either and were recurrently twinned; however, disorder problems involving solvent were not found, and consequently, the refinement was a little better.

Hydrogen atoms of the organic ligands for both compounds were situated at their calculated positions.

Calculations were carried out with SMART software (for data collection and data reduction) and SHELXTL.[21] CCDC xxx-xxx contains the supplementary crystallographic data for this paper. These data can be obtained free of charge from The Cambridge Crystallographic Data Center via www.ccdc.cam.ac.uk/data_request/cif.

X-ray Powder Diffraction Data. X-ray powder diffraction (PXRD) measurements were performed with a Bruker D8 diffractometer in the $\theta-\theta$ mode using nickel-filtered Cu Kα (λ = 1.5418 Å) radiation. The best counting statistics were achieved using a scanning step of 0.02° and was taken between 5° and 40° Bragg angles with an exposure time of 2 s per step.

X-ray Powder Data Refinements. The Pawley profile-fitting procedure (2θ = 5−40°) using the FullProf Suite software package[22] was performed to refine the cell and peak profile parameters as well as those of the background, peak asymmetry, and zero shift.

The X-ray powder thermodiffractometry study was carried out with a Siemens D-5000 powder diffractometer (Cu Kα radiation, λ = 1.5418 Å) equipped with a high-temperature HTK1200 Anton Paar camera mounted on a $\theta-2\theta$ goniometer. Data were scanned over the range 2θ = 5−40 with 2θ step size = 0.04 and counting time = 2 s/step. The sample heating rate was 10 °C min⁻¹ in the 25−220 °C temperature range.

5959

dx.doi.org/10.1021/ic102472u |*Inorg. Chem.* 2011, 50, 5958–5968

Scheme 1. Hydrolysis of Succinylsalicylic Acid
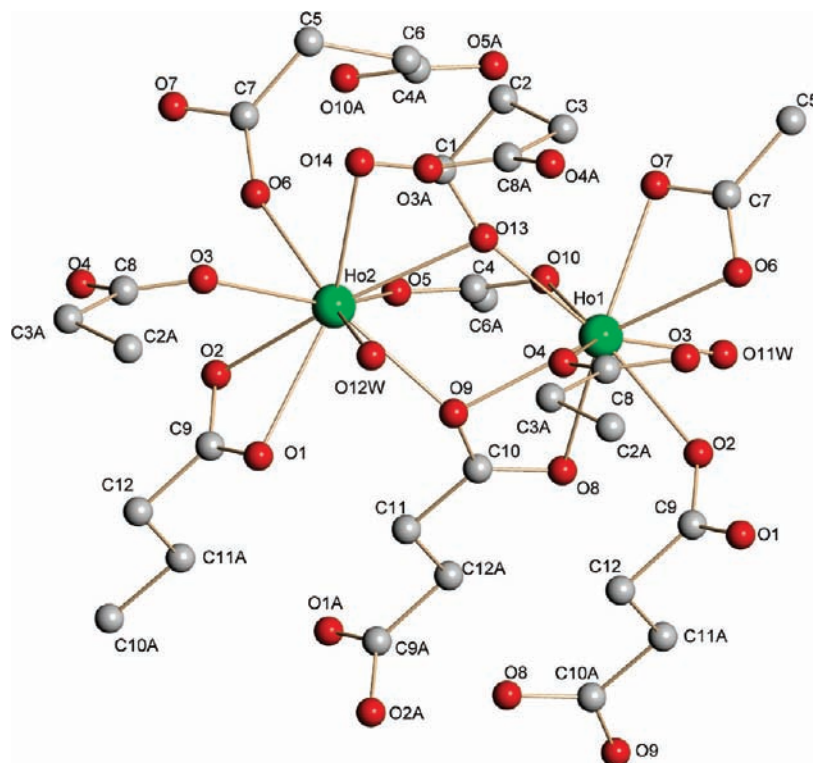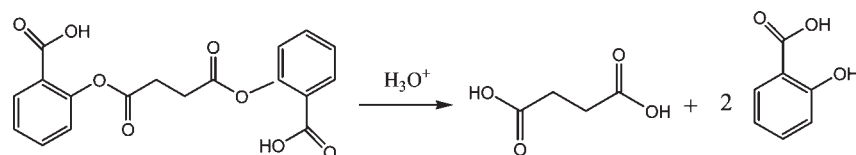
Figure 1. Coordination environment of Ho(III) ions in **1**. Hydrogen atoms were omitted for clarity.

Infrared Spectroscopy. The IR spectra were recorded from KBr pellets in the range 4000−250 cm^{-1} on a Perkin-Elmer spectrometer.

Thermal Analysis. Thermogravimetric and differential thermal analyses (TGA/DTA) were performed using a SEIKO TG/DTA 320 apparatus in the temperature range 25−800 °C in air atmosphere (flow of 100 mL min^{-1}) at a heating rate of 10 °C min^{-1}.

Thermogravimetric Analysis-Mass Spectrometry (TGA-MS). Characterization by mass spectrometry was performed using a quadrupolar mass spectrometer for gas analysis, model THERMOSTAR, coupled to a simultaneous TG/DTA analyzer SDT Q600 apparatus in the temperature range 25−500 °C in argon atmosphere (flow of 100 mL min^{-1}) at a heating rate of 10 °C min^{-1}.

Crystal Structure Description. *Compound 1.* Hydrolysis of the succinylsalicylic acid takes place during the synthesis process, (see Scheme 1), generating the succinic and salicylic acids in the reaction medium.

The pH value of the reaction mixture is enough for deprotonation of both acids; thus, a competition between these ligands should occur. The flexible succinate anion seems to exhibit more effective Lewis basic characteristics and coordination ability than the salicylic one since the resultant framework includes only the succinate ligand.

In the asymmetric unit of compound **1** there are two crystallographically nonequivalent Ho(III) cations; each one has a coordination number of 9 (see Figure 1), and the coordination polyhedra can be described as a monocapped square antiprism. In each Ho(III) coordination sphere, eight oxygen atoms come from carboxylate groups while the ninth belongs to a coordinated water molecule.

There are three crystallographically nonequivalent succinate anions; one of them adopts a trans conformation with a dihedral CCCC angle of 171(2)° and a distance between the α and ω carbon atoms of 3.79(4) Å. The anion extends approximately in the [10−1] direction and acts as chelate bridge by its two carboxylate groups. Thus, this ligand is a $\eta^2\mu_2$-$\eta^2\mu_2$ linker and connects four holmium ions.

Both remaining succinate anions coordinate through a chelate-bridge mode by one carboxylate group and in a bidentate-bridge mode by the other one. In this way, these anions are also $\eta^2\mu_2$-$\eta^2\mu_2$ linkers, exhibiting a gauche conformation with dihedral angles of 65(3)° and −64(3)°, with 3.12(3) and 3.21(4) Å being the distances between the α and the ω carbon atoms, respectively. These ligands extend along the [001] direction (see Figure 2).

The secondary building unit (SBU) is constituted by chains of edge-sharing coordination polyhedra running along to the [100] direction (see Figure 2). Parallel to this direction, two sets of channels are determined. The smaller one is empty and has a transversal area of ~25.6 Å^2, while the bigger one is partially occupied by 1/3 of the salicylic acid molecules and has a transversal area of ~113.4 Å^2 (see Figure 2).

Figure 2. Perspective views of the *bc* (a) and *ab* (b) planes of **1**.

Figure 3. Coordination environment of Ho(III) ions in **2**. Hydrogen atoms were omitted for clarity.

The presence of the aromatic molecule was confirmed by elemental analysis with values for C = 22.88% and H = 2.56% in very good agreement with the calculated ones of 22.61% and 2.36%, respectively. This result led us to propose the formula $[Ho_2(C_4H_4O_4)_3(H_2O)_2]\cdot 0.33\text{-}(C_7H_6O_3)$. The atomic positions of the aromatic molecule could not be determined, since the continuous electron density found all along the

channels showed no resolvable positional disorder (see Experimental Section).

Compound **2**. It is isostructural to other REE succinates such as those of Er,[23] Gd,[24] Eu,[25] Nd,[26] and Ce,[27] but this structural type has not been reported for Ho yet, its molecular formula being $[Ho_2(C_4H_4O_4)_3(H_2O)_2]$.

The structure is very similar to that of compound **1** in terms of their constituent units. There are two crystallographically nonequivalent Ho(III) ions, both exhibiting the same coordination environment formed by nine oxygen atoms (one of them belongs to a coordinated water molecule, and the remaining ones are from carboxylate groups, see Figure 3). There are three types of succinate anions similar to those described for compound **1**, the only differences being the values of the dihedral angles. The trans succinate ligand has a dihedral angle of $177(2)°$, and the torsion angles of both gauche anions are $-69(2)°$ and $-90(2)°$. The distances between the α and the ω carbon atoms in these three types of succinate anions are $3.84(4)$, $3.07(3)$, and $3.21(3)$ Å, respectively. The coordination modes of each ligand are similar to those found for the corresponding ligands of compound **1**. The trans conformer extends in the $[010]$ direction, and both gauche succinates run parallel to the $[001]$ direction (see Figure 4).

SBU in **2** also consists of chains of coordination polyhedra joined by edges that extend parallel to the $[100]$ direction.

An important structural difference between compounds **1** and **2** relies on the disposition of the organic linkers in the framework. As a result, channels of different sizes and geometries are determined in each network. At this point, it is interesting to note that **1** has channels with the biggest transversal area among known REE succinates, resulting in a free void volume of 215 Å³ per unit cell that represents 21.5% of the cell volume (calculated value with the PLATON program[28]). The same calculation has been performed for **2** and for the 3D Ho(III) succinate framework previously reported[11] ($C2/c$ space group; named compound **0** from now on); both unit cells contain no residual solvent accessible voids. Similar calculation has also been carried out for the α- and β-polymorphs of an Yb−succinate frameworks,[12] and the same result has been found. Thus, the compound **1** framework represents the most open one found in hydrothermally obtained REE succinates.
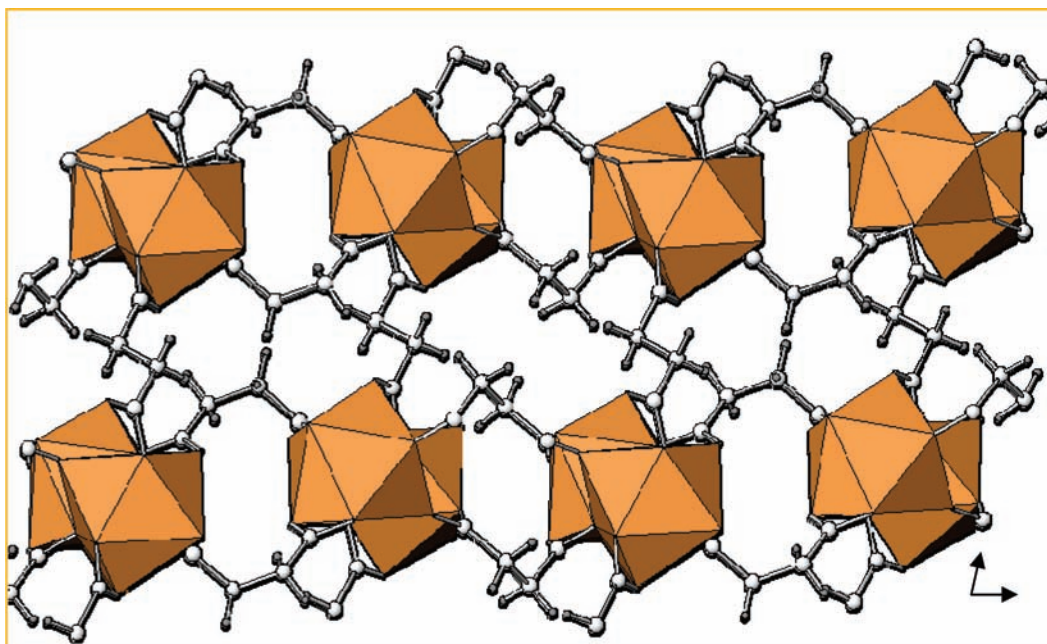
Figure 4. Perspective view of the *bc* plane of **2**.

Table 2. Tuning the Synthesis Conditions

test no.	Ho:Succ:benzene (Bz) (mmol)	composition of the reaction mixture	temp. (°C)	time (days)	products
0	0.5:0.75:0	10 mL of H_2O, pH = 5.5 (TEA)	160	3	**0**
1	0.5:0.75:2.23	9.8 mL of H_2O, 0.2 mL of Bz, pH = 5.5 (TEA)	160	3	**0** (majority) + **2** (impurity)
2	0.5:0.75:11.14	9 mL of H_2O, 1 mL of Bz, pH = 5.5 (TEA)	160	3	**0** + **2** + unknown impurity
3	0.5:0.75:33.43	7 mL of H_2O, 3 mL of Bz, pH = 5.5 (TEA)	160	3	**1·Bz** + unknown impurity
4	0.5:0.75:50.14	5.5 mL of H_2O, 4.5 mL of Bz, pH = 5.5 (TEA)	160	3	pure compound **1·Bz**

Role of the Aromatic Molecules. In order to study the role of the aromatic molecule included into the main channels of **1** we performed its synthesis replacing the succinylsalicylic acid by a combination of succinate ligand and different aromatic molecules. In this way, the reaction mixture consisted of $Ho(NO_3)_3 \cdot 5H_2O$, succinic acid, water, TEA, and one of the following aromatic compounds: benzene (Bz), pyridine (Py), toluene (Tol), salicylic acid (Slc), or acetylsalicylic acid (Ac.Slc). The temperature was fixed at 160 °C, and several reaction times were tested in order to obtain, as pure phases, compounds with the **1** framework. Besides, a synthesis without any aromatics and maintaining constant all variables has been also carried out (named from now on as test no. 0, see Figure S2 in the Supporting Information).

The step-by-step comprehensive study and tuning of the synthesis conditions were carried out using benzene, and then, when the conditions for the obtaining of a pure compound with **1** framework were found, such conditions allowed for rapid optimization of the synthesis with the other aromatics.

Table 2 shows the different steps for tuning the synthesis conditions of compound **1·Bz** whereas Figure 5 displays the corresponding PXRD patterns. Table 3 summarizes the optimized synthesis conditions for all the aromatic molecules tested. The corresponding PXRD patterns are shown in Figure 6.

According to the results listed in Table 2, compound **0** is obtained as a pure phase when benzene is absent. The low content of benzene (tests 1 and 2) in the initial mixture induces formation of compound **2** (apart from compound **0**) as it can be observed in the PXRD pattern

(see Figure 5), allowing us to assign it a SDA role. In such conditions, a template effect during formation of compound **2** is disregarded not only for the absence of the aromatic molecules but also for the resultant small size of the main channels.

On the other hand, as benzene content increases, a new structural effect is observed toward formation of the **1** framework (tests 3 and 4). In this case, the presence of this molecule trapped inside the channels has been confirmed by elemental analysis (see Supporting Information), indicating that it behaves as a true template.

Considering the review of Tanaka and Kitagawa on template effects in porous coordination polymers,[29] this effect can be primary or secondary. The primary template effect occurs during the synthesis process when the organic guest molecule is self-included into the host framework by noncovalent interactions acting as a placeholder, thus preventing interpenetration of the open framework. The secondary template effect is a dynamic process that occurs when appropriate guest molecules act as templates and induce reversible structure transformations.

PXRD data confirm that the different aromatics tested render as pure phases compounds that share identical hybrid framework with **1**, except for toluene. As in the case of benzene, salicylic and acetylsalicylic acids behave as templates since the corresponding moieties hosted in **1·Slc** and **1·Ac.Slc** networks can be satisfactorily assessed from elemental analysis. On the contrary, these measurements are unable to determine undoubtedly the presence of pyridine in the respective reaction product, thus suggesting a SDA role for the aromatic molecule. Perhaps, this fact is somehow expected taking into account the chemical differences
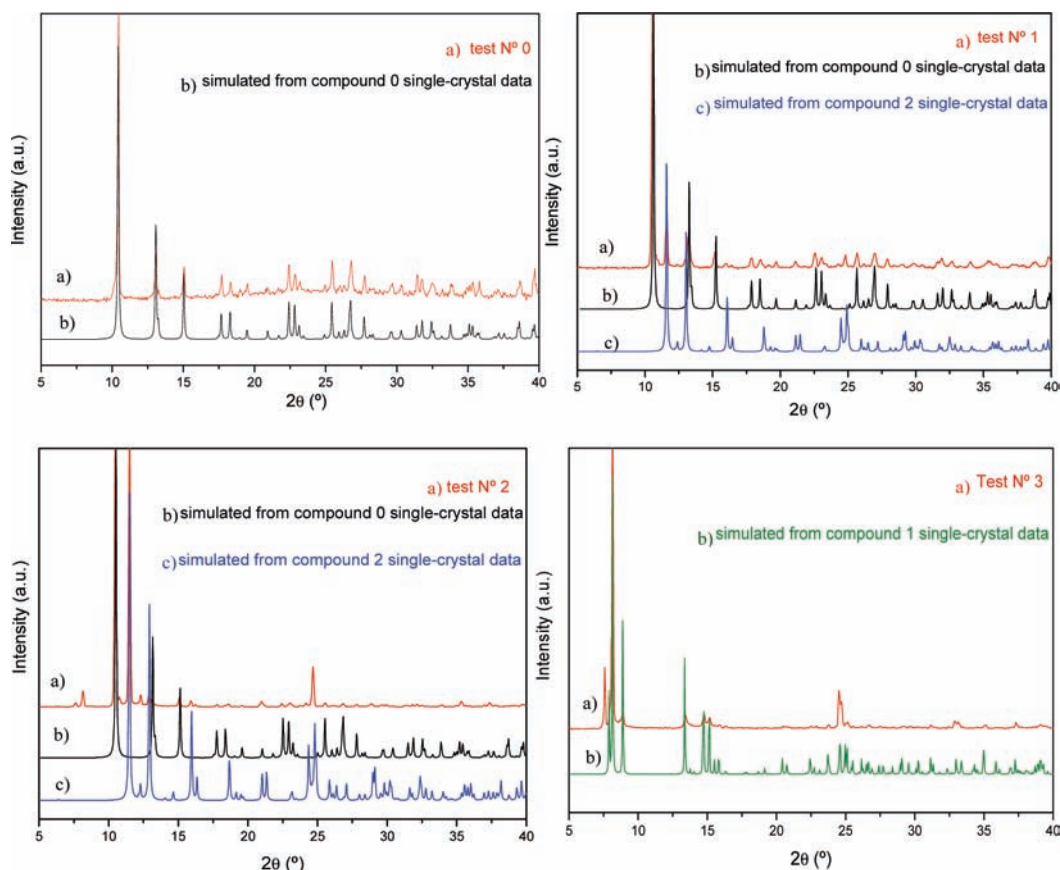
Figure 5. Experimental PXRD patterns of the products stated in Table 2 in comparison with the corresponding simulated ones.

Table 3. Tuning the Synthesis Conditions Organized by the Aromatic Molecule Used

aromatic molecule (Ar.Mol)	Ho:Succ:Ar.Mol (mmol)	composition of the reaction mixture	temp. (°C)	time (days)	products[a]
Bz	0.5:0.75:50.14	5.5 mL of H_2O, 4.5 mL of Bz, pH = 5.5 (TEA)	160	3	**1·Bz**
Py	0.5:0.75:61.82	5 mL of H_2O, 5 mL of Py, pH = 5.5 (TEA)	160	4	**1-Py**
Tol[b]	0.5:0.75:46.96	5 mL of H_2O, 5 mL of Tol, pH = 5.5 (TEA)	160	3, 4	**0 + 1·Tol**
Slc	0.5:0.75:5	10 mL of H_2O, 690 mg of Slc, pH = 5.5 (TEA)	160	4	**1**
Ac.Slc	0.5:0.75:5	10 mL of H_2O, 900 mg of Ac.Slc, pH = 5.5 (TEA)	160	4	**1·Ac.Slc**

[a] The corresponding formulas are given in the Thermal Analysis section and the Supporting Information (Elemental Analysis data). [b] Comparison of simulated and experimental XRD powder pattern is shown in Figure S3, Supporting Information.

between pyridine and the rest of the aromatics employed such as donor atoms, basicity, etc. On the other hand, the elemental analysis data for **1-Py** are consistent with water molecules occupying the cavities.

The results displayed in Table 3 indicate that the amounts of benzene and pyridine necessary for obtaining a pure compound with **1** framework are much bigger than in the case of salicylic and acetylsalicylic acids. The low solubility in water of those organic liquids could explain this fact. Both syntheses are biphasic, and the benzene or the pyridine reactants have to be in great excess with respect to the succinate to achieve an effective concentration in the reaction medium, which is controlled by the partition coefficient at the synthesis temperature. Moreover, a potential template activity for pyridine at higher concentrations could be considered.

It is remarkable that using toluene, a pure compound with **1** frame-work, could not be obtained, as the minor phase is always in coexistence with compound **0** (see Figure S3 in Supporting Information), showing its less effective behavior as a template.

It is worth analyzing the influence of the in-situ generation of the template molecule. When compound **1** is synthesized using succinylsalicylic acid (see Experimental Section), only a 2:1 salicylic acid:succinate ligand molar ratio is necessary, whereas employing a reactant mixture that contains the constituent ligands as independent molecules requires a higher content of the aromatics. However, this methodology does not always lead to formation of the same compound obtained by the in-situ-generated ligands, as reported in previous studies.[17b] The above considerations are also valid for compound **2** since the SDA molecule (i.e., benzene) added as an independent species has to be in greater excess with respect to the succinate ligand (see tests 1 and 2 in Table 2) in comparison to salicylic acid generation in situ.

Finally, attempts employing naphthalene were also tried without success. The importance of the complementary relationship between the selected template and the features of the ligand is evident; that is, the template has to fit into the available space and also has to create the specific favorable interactions that stabilize the structure.[30] In particular,
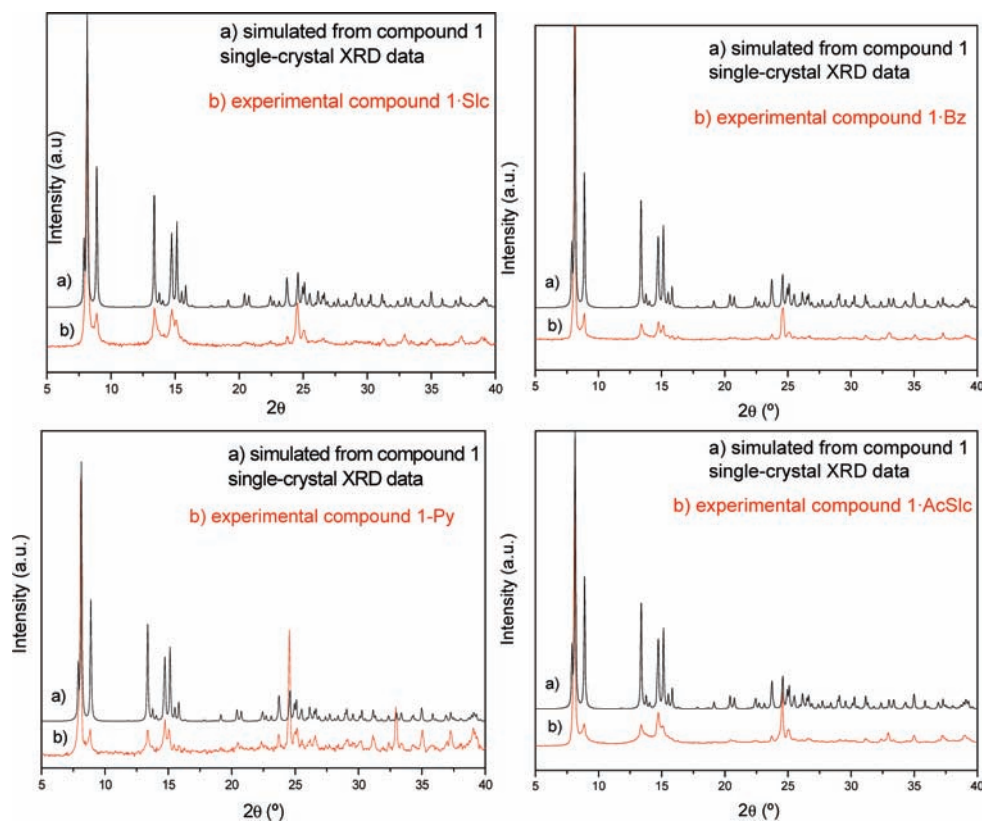
Figure 6. Experimental PXRD patterns of the products listed in Table 3 in comparison with the corresponding simulated one from **1** single-crystal data.

the succinate-based framework of compound **1** is considerably "stretched" to its maximum capacity, and a bigger template molecule cannot be included inside. Then, is it possible to obtain other Ln—MOFs employing longer dicarboxylic acids such as glutaric, adipic, pimelic, and so on, by means of the template role of naphthalene, anthracene, phenanthrene, and other larger aromatic molecules...? In this sense, the primary template effect can not only play an integral role in the solid-state assembly process itself but also determine the shape and chemical superficial properties of the pores.[29] Further research will be done in order to obtain deeper knowledge on the template effect of aromatics on obtaining 3D MOFs.

Topological Study. Most metal—organic framework structures belong to known prototypes in metallic or binary inorganic solids, which can usually be described as 3-, 4- or 6-connected nets, for example, 3-connected (6,3), (8,3), (10,3), and (12,3) nets, 4-connected diamond, $CdSO_4$, quartz, moganite, and $SrAl_2$ nets, and 6-connected α-Po and β-Sn nets,[31] with the three most preferred topological motifs being the **dia**, **pcu**, and **srs**.[32]

The succinate ligand is flexible and versatile since it can exhibit different coordination modes and conformations, allowing development of new structures and diverse topologies. For this reason, a topological analysis using the TOPOS[33] program was performed on compounds **1** and **2**, comparatively with compound **0**.[11] This study has been carried out in order to analyze whether the different connectivity in the hydrothermally obtained 3D-REE succinate frameworks gives different network topologies.

Due to the fact that compounds **0**, **1**, and **2** are 3D frameworks in which the SBUs are conformed by chains of edge-sharing $[HoO_9]$ polyhedra, the simplest topological depictions can be done regarding only the packing of such SBUs. In this sense, the framework is visualized as a periodic arrangement of 1D inorganic units and the organic ligands are only linking them. The description of MOF geometry in terms of
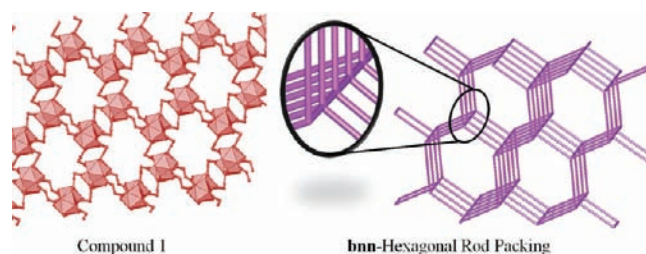

Figure 7. Comparison of the crystal structure of compound **1** (left) with the topological representation based on the **bnn** hexagonal rod packing.

linked rod-shaped SBUs is fundamental to the rationalization and prediction of MOF net topologies.[34,35]

From this point of view, compound **1** can be described as a uninodal net with 5-connected nodes conforming rods that extend along the [100] direction. The rods are linked by the succinate ligands to produce a typical **bnn** net with a hexagonal parallel rod packing (see Figure 7), Point Schläfli Symbol $\{4^6.6^4\}$.

When the same analysis is performed on compound **0**, the obtained result is also a uninodal **bnn** net, with rods running along the [010] direction; however, in this simplified net, the geometry of the 5-connected nodes is square pyramidal, different from the trigonal bipyramide exhibited by the 5-connected nodes in **1** (see Figures 7 and 8(left)). In compound **0** net, the nodes not only connect to each other inside a rod but also connect three rods disposed in a "square" array, whereas in **1**, the rods are located at 120° each other in a typical hexagonal array.

For compound **2**, the simplified net is binodal with nodes 4,5-connected, the Point (Schläfli) symbol being $\{4^2.6^3.8\}\{4^2.6^7.8\}$. However, this binodal net, as well as the compound **0** one, can be assimilated
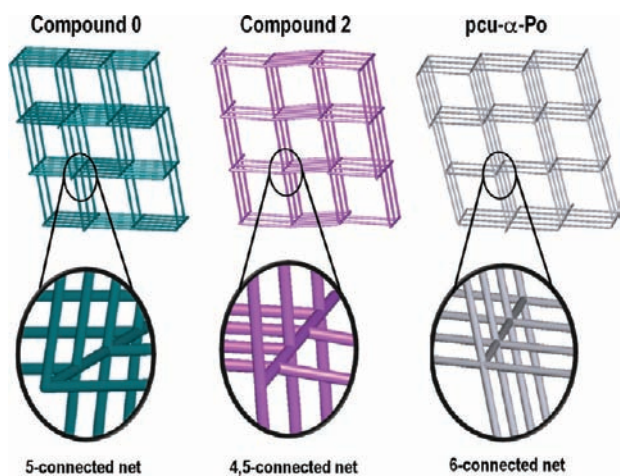
Figure 8. Comparison of the simplified nets of compounds **0** (left) and **2** (center) with the ideal square rod packing type **pcu**-α-Po.
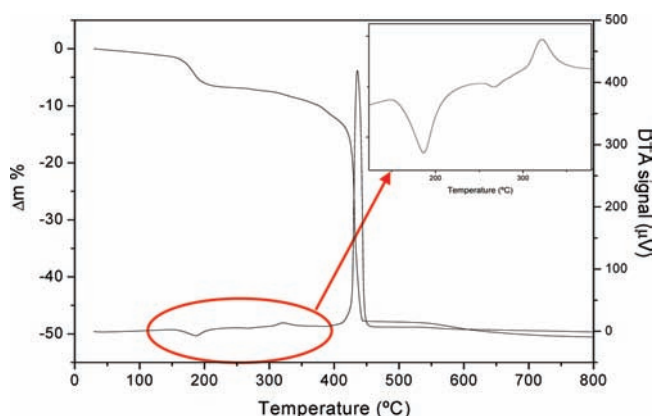

Figure 9. TGA-DTA curves for compound **1**. (Inset) Zoom of the DTA curve in the 120–380 °C range.

to the ideal **pcu**-α-Po square rod packing. In spite of the different connectivity of the nodes in the rods (5-connected in **0**, 4,5-connected in **2**, and 6-connected in **pcu**), the three simplified nets visualized along the direction parallel to the rods are very similar. The differences with **pcu** are more evident along the other two crystallographic directions, where the dissimilar connectivity of the nodes leads to less symmetric packings. Thus, the simplified nets of compounds **0** and **2** can be considered as pseudosquare rod packing.

From a chemical point of view, when the focus is on the skeletal frameworks of the Ho—succinates, compounds **0**, **1**, and **2** can be considered as pseudopolymorphs since they share the formula $[\text{Ho}_2(\text{C}_4\text{H}_4\text{O}_4)_3(\text{H}_2\text{O})_2]$. Referring to the total composition, they only differ in the channel contents, that is, water molecules in **0** or salicylic acid molecules in **1**, whereas they are empty in **2**. However, these minor differences are important; not only channels of different sizes are determined depending on the inclusion or not of a certain molecule but also the resultant frameworks present different structures and topologies.

Thermal Analysis. TGA and DTA curves of compound **1** are shown in Figure 9, whereas the corresponding curves for compounds **1·Bz**, **1-Py** and **1·Ac.Slc** are gathered in Figures S4–S6, Supporting Information.

For compound **1**, the first weight loss in the TGA curve is about 5.85% and is associated with a DTA endothermic peak centered at
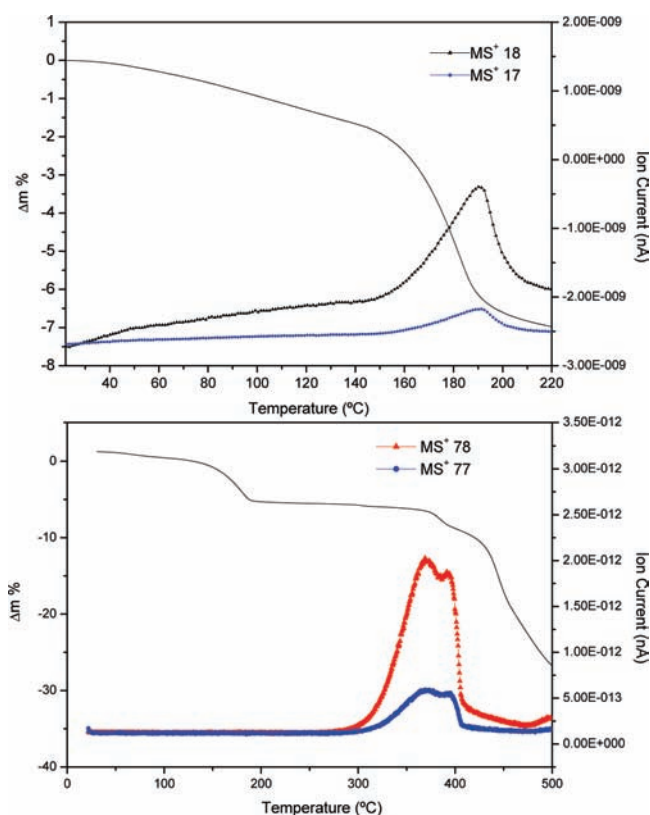
Figure 10. TGA curve for compound **1·Bz** along with the corresponding ion current detected in the 20–220 °C range (top) and in the 20–500 °C range (bottom).

Table 4. Refined Cell Parameters for Compounds 1, 1·Bz, 1-Py, and 1·Ac.Slc and Reliability Factors of the Pawley Fittings

	1	**1·Bz**	**1-Py**	**1·Ac.Slc**
a (Å)	7.6315(5)	7.625(1)	7.640(1)	7.653(1)
b (Å)	11.999(1)	11.981(2)	12.011(1)	11.959(2)
c (Å)	12.157(1)	12.131(1)	12.113(1)	11.990(3)
α (deg)	67.552(4)	67.498(8)	67.143(6)	67.79(1)
β (deg)	89.873(7)	89.93(1)	89.881(6)	90.65(1)
γ (deg)	80.518(5)	80.59(2)	80.861(7)	80.94(2)
R_{wp} (%)	11.9	7.1	7.6	8.2

~180 °C. The second process begins at ~260 °C and extends until ~400 °C with a mass decay of 5.5%. This event is denoted by a complex signal in the DTA curve composed by an exothermic peak centered at ~320 °C along with a previous weak endothermic one; these peaks could be related with removal of the template molecule from the framework. Decomposition of the succinate ligand is related to a strong exothermic DTA signal at 435 °C, the cubic Ho_2O_3 (PDF card 43-1018)[36] being the final product of the pyrolysis. The weight change for the whole process is −50.4%, consistent with the calculated value of −50.24%.

For **1·Bz**, **1-Py** and **1·Ac.Slc**, the corresponding weight losses for the whole process are 50.0%, 49.43%, and 49.2%, respectively, which are in very good agreement with the theoretical values of 49.75%, 49.84%, and 50.2% for the corresponding formulas $[\text{Ho}_2(\text{C}_4\text{H}_4\text{O}_4)_3(\text{H}_2\text{O})_2]\cdot0.5\text{-}(\text{C}_6\text{H}_6)$, $[\text{Ho}_2(\text{C}_4\text{H}_4\text{O}_4)_3(\text{H}_2\text{O})_2]\cdot2\text{H}_2\text{O}$, and $[\text{Ho}_2(\text{C}_4\text{H}_4\text{O}_4)_3(\text{H}_2\text{O})_2]\cdot0.25(\text{C}_9\text{H}_6\text{O}_4)$. These stoichiometries are consistent with

the elemental analysis results (see Supporting Information). The succinate decomposition processes are denoted by strong exothermic peaks centered in all cases at ∼435 °C in the DTA curves (see Figures S4–S6, Supporting Information).

In the case of **1-Py**, the first mass loss of 5.5% occurs from room temperature to 100 °C and is associated with evacuation of the hydration water molecules (calculated value 4.82%), while the second weight loss of 4.95% (calculated value 4.82%) corresponds to removal of both coordination water molecules. In the DTA curve, two endothermic peaks appear at ∼60 and 170 °C, which are associated with these events (see Figure S5, Supporting Information).

According to these results, the compound with the higher content of aromatic molecule is **1·Bz**; thus, such compound was selected for a coupled thermogravimetric analysis mass spectrometry (TGA-MS) study to determine the nature of the evolved decomposition gases.

Surprisingly, only ions $m/z = 18^+$ and 17^+ were detected, and no evidence of the benzene molecular ion or its fragmentation products
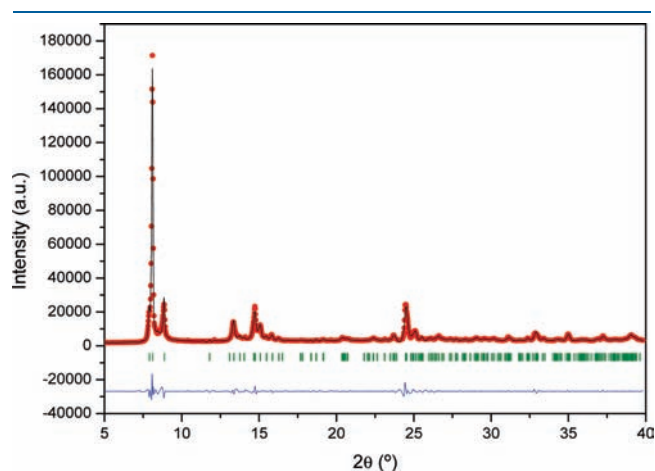
Figure 11. Pawley refinement for compound **1·Bz**. Experimental data (red), simulated pattern (black), difference (blue), and Bragg reflections (green).

appeared in the 20–220 °C temperature range. In this way, the first step of the TGA curve corresponds to loss of the coordinated water molecules. The TGA-MS curves are shown in Figure 10(top).

Then, a TGA-MS measurement was performed up to 500 °C for compound **1·Bz** in order to confirm the presence of the benzene molecule as a hosted species. Determination of the corresponding elimination temperature would help to infer the structural importance that this molecule has in the structure. As can be seen from Figure 10-(bottom), the characteristic peaks of the mass spectrum of benzene corresponding to ions $m/z = 78^+$ and 77^+ appear between 300 and 400 °C. This fact is associated with the second weight loss that occurs in the same temperature range. Consequently, once the template molecule is evacuated, the framework immediately decomposes, demonstrating the strong stabilization effect of the template that contributes to maintenance of the host structure.

X-ray Powder Diffraction Study. Taking into account that only the structure of compound **1** was solved by single-crystal X-ray diffraction, the isostructural character of all compounds is determined by comparison of the corresponding powder XRD patterns. To refine the cell parameters at room temperature of the compounds under study, Pawley profile-fitting procedures (see Experimental Section) were performed (Table 4), and the corresponding Pawley refinements are shown in Figures S7–S10, Supporting Information. As an example, the results corresponding to the compound **1·Bz** are gathered in Figure 11.

On the other hand, in order to study the stability of compound **1·Bz** when coordinated water molecules are eliminated, an X-ray thermodiffractometry study has been performed in the 20–220 °C range, and the results are shown in Figure S11, Supporting Information. As can be seen, the structure does not collapse upon dehydration even though some modifications and a loss of crystallinity are observed. Besides, an inversion of the relative intensities of the two first peaks corresponding to the (010) and (011) *hkl* planes is observed. The initial structure tends to be recovered when the sample returns to room temperature, denoted by the reset of the aforementioned relative intensities (see Figures 12 and S11, Supporting Information).

Infrared Spectroscopy. Figure 13 shows the IR spectra of compounds **1**, **1·Bz**, **1-Py**, and **1·Ac.Slc**, which are almost identical since the aromatic molecules are present in a very low amount in the
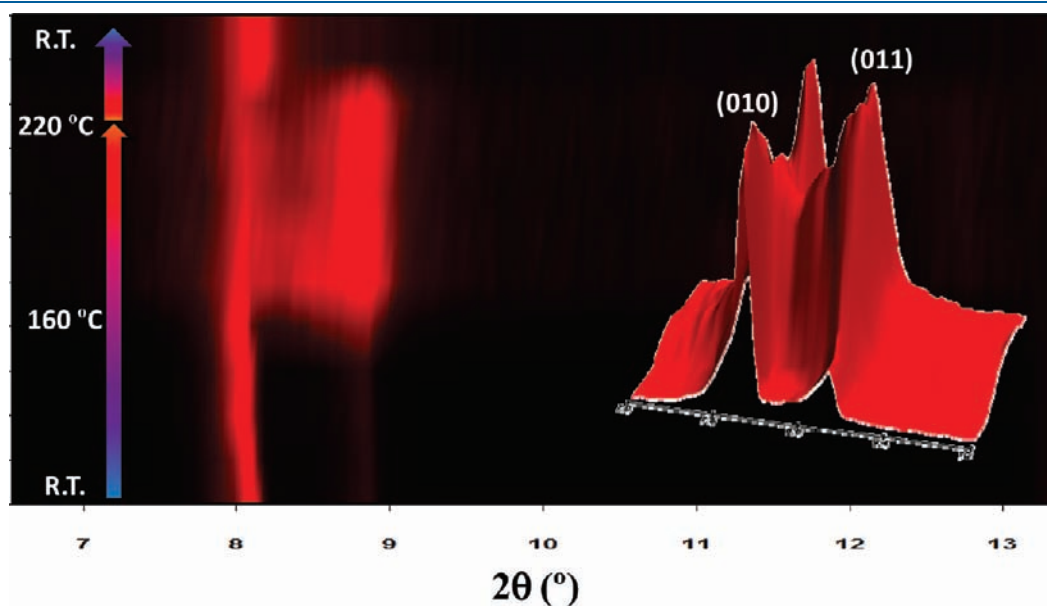
Figure 12. 2D contour graph corresponding to the intensities of the (010) and (011) reflections as a function of temperature for compound **1·Bz**. (Inset) 3D representation.
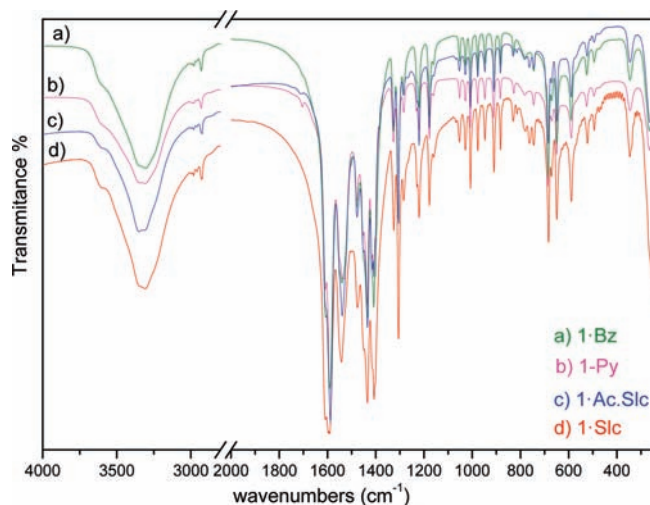
Figure 13. Infrared spectra of compounds **1**, **1·Bz**, **1-Py**, and **1·Ac.Slc**.

structures. On the contrary, if such spectra are compared with that reported in ref 11 for compound **0**, a major degree of splitting and the appearance of new bands are observed in the former cases attributed to the existence of two crystallographically nonequivalent gauche succinate anions in the case of **1** instead of only one in the case of compound **0**.

The OH-stretching mode is observed as a broad band centered at $\sim$3340 cm^{-1}, while the C—H stretching one is located around 2930 cm^{-1} as weak bands. The OCO antisymmetric stretching mode is assigned to three very strong bands located at 1605, 1595, and 1540 cm^{-1}, the first two bands being associated to the bidentate carboxylate groups while the third band is to the chelate-bridge ones. The CH$_2$ bending mode appears, as in the case of other Ho—succinate frameworks, in the 1480—1400 cm^{-1} region. The Ho—O stretching mode is assigned to three bands located at 590, 520, and 490 cm^{-1}, in agreement with our previous vibrational studies on other REE—succinate MOFs.[12,37]

CONCLUSIONS

Two novel 3D holmium MOF compounds have been obtained by hydrolysis of the succinylsalicilic acid allowing in-situ generation of the succinate ligand. Compound **1** exhibits a novel structure induced by the primary template effect of the salicylic acid molecules hosted in the channels. The framework has channels with the biggest transversal area reported for REE—succinate MOFs; it includes the aromatic molecules in low quantity. Replacing succinylsalycilic acid by mixtures of succinate ligand and different aromatic molecules, compounds with **1** framework are obtained, confirming the primary template effect of the aromatic molecules. From the structural and topological analysis performed, we can conclude that in the Ho—succinate 3D frameworks such molecules act in two different ways: as purely structure-directing agents (salicylic acid and benzene in formation of **2** and pyridine in formation of **1-Py**) and as templates (salicylic acid, benzene, and acetylsalicylic acid in formation of **1**, **1·Bz**, and **1·Ac.Slc**).

A comprehensive study following a design of synthesis methodology to obtain the desired compounds suggests that the role of the aromatics varies from SDA to template as their amounts increase in the reaction mixture. In this way, this work contributes to the increasing knowledge of the structure-directing and template effects in MOFs.

ASSOCIATED CONTENT

ⓢ Supporting Information. X-ray crystallographic files in CIF format of compounds **1** and **2**. This material is available free of charge via the Internet at http://pubs.acs.org.

AUTHOR INFORMATION

Corresponding Author
*E-mail: amonge@icmm.csic.es.

REFERENCES

(1) Rowsell, J.; Yaghi, O. *Microporous Mesoporous Mater.* **2004**, *73*, 3.
(2) Maji, T.-K.; Uemura, K.; Chang, H.-C.; Matsuda, R.; Kitagawa, S. *Angew. Chem., Int. Ed.* **2004**, *43*, 3269.
(3) (a) Ghosh, S. K.; Zhang, J. -P.; Kitagawa, S. *Angew. Chem., Int. Ed.* **2007**, *46*, 7965. (b) Ghosh, S. K.; Bureekaew, S.; Kitagawa, S. *Angew. Chem., Int. Ed.* **2008**, *47*, 3403. (c) Horike, S.; Tanaka, D.; Nakagawa, K.; Kitagawa, S. *Chem. Commun.* **2007**, 3395. (d) Maji, T. K.; Mostafa, G.; Matsuda, R.; Kitagawa, S. *J. Am. Chem. Soc.* **2005**, *127*, 17152.
(4) (a) Horcajada, P.; Serre, C.; Vallet-Regi, M.; Sebban, M.; Taulelle, F.; Férey, G. *Angew. Chem., Int. Ed.* **2006**, *45*, 5974. (b) Horcajada, P.; Chalati, T.; Serre, C.; Gillet, B.; Sebrie, C.; Baati1, T.; Eubank, J. F.; Heurtaux, D.; Clayette, P.; Kreuz, C.; Chang, J.-S.; Hwang, Y. K.; Marsaud, V.; Bories, P. N.; Cynober, L.; Gil, S.; Férey, G.; Couvreur, P.; Gref, R. *Nat. Mater.* **2010**, *9*, 172.
(5) (a) Hermes, S.; Schroder, F.; Amirjalayer, S.; Schmid, R.; Fischer, R.-A. *J. Mater. Chem.* **2006**, *16*, 2464. (b) Allendorf, M. D.; Houk, R. J. T.; Andruszkiewicz, L.; Talin, A. A.; Pikarsky, J.; Choudhury, A.; Gall, K. A.; Hesketh, P. J. *J. Am. Chem. Soc.* **2008**, *130*, 14404.
(6) (a) Cundy, C. S.; Cox, P. A. *Microporous Mesoporous Mater.* **2005**, *82*, 1. (b) Davis, M. E.; Lobo, R. F. *Chem. Mater.* **1992**, *4*, 756.
(7) Bajpe, S. R.; Kirschhock, C. E. A.; Aerts, A.; Breynaert, E.; Absillis, G.; Parac-Vogt, T. N.; Giebeler, L.; Martens, J. A. *Chem.—Eur. J.* **2010**, *16*, 3926 and references therein.
(8) (a) Ghoshal, D.; Kumar Ghosh, A.; Mostafa, G.; Ribas, J.; Ray Chaudhuri, N. *Inorg. Chim. Acta* **2007**, *360* (5), 1771. (b) Guillou, N.; Livage, C.; Férey, G. *Eur. J. Inorg. Chem.* **2006**, *24*, 4963. (c) Guillou, N.; Livage, C.; Van Beek, W.; Noguès, M.; Férey, G. *Angew. Chem., Int. Ed.* **2003**, *42* (6), 644. (d) Forster, P. M.; Cheetham, A. K. *Angew. Chem., Int. Ed.* **2002**, *41* (3), 457. (e) Vaidhyanathan, R.; Natarajan, S.; Rao, C. N. R. *Inorg. Chem.* **2002**, *41* (20), 5226. (f) Burbank, A. R.; O'Sullivan, M. C.; Guillou, N.; Livage, C.; Férey, G.; Stock, N.; Cheetham, A. K. *Solid State Sci.* **2005**, *7* (12), 1549. (g) Forster, P. M.; Stock, N.; Cheetham, A. K. *Angew. Chem., Int. Ed.* **2005**, *44* (46), 7608. (h) Forster, P. M.; Burbank, A. R.; Livage, C.; Férey, G.; Cheetham, A. K. *Chem. Commun.* **2004**, *10* (4), 368.
(9) (a) Serpaggi, F.; Ferey, G. *Microporous Mesoporous Mater.* **1999**, *32*, 311. (b) Fleck, M. *Z. Kristallogr. NCS* **2002**, *217*, 569. (c) Li, H. *Acta Crystallogr., Sect. E* **2007**, *63* (3), 84. (d) Sun, J.; Zheng, Y.-Q.; Lin, J. L. *Z. Kristallogr. NCS* **2004**, *219*, 99. (e) Nika, W.; Pantenburg, I.; Meyer, G. *Acta Crystallogr., Sect. E* **2005**, *61*, 138. (f) Cui, G.-H.; Li, J.-R.; Zhang, R.-H.; Bu, X.-H. *J. Mol. Struct.* **2005**, *740*, 187. (g) Zhou, Y.-F.; Jiang, F.-L.; Yuan, D.-Q.; Wu, B.-L.; Hong, M.-C. *J. Mol. Struct.* **2005**, *743*, 21.
(10) Perles, J.; Iglesias, M.; Ruiz-Valero, C.; Snejko, N. *J. Mater. Chem.* **2004**, *14*, 2683.
(11) Bernini, M. C.; Brusau, E. V.; Narda, G. E.; Echeverría, G. E.; Pozzi, C. G.; Punte, G.; Lehmann, C. W. *Eur. J. Inorg. Chem.* **2007**, *5*, 684.

(12) Bernini, M. C.; Gándara, F.; Iglesias, M.; Snejko, N.; Gutierrez-Puebla, E.; Brusau, E. V.; Narda, G. E.; Monge, M. A. *Chem.—Eur. J.* **2009**, *15* (19), 4896.

(13) Feller, R. K; Forster, P. M.; Wudl, F.; Cheetham, A. K. *Inorg. Chem.* **2007**, *46*, 8717.

(14) (a) Yang, S.-Y.; Long, L.-S.; Huang, R.-B.; Zheng, L.-S.; Ng, S. W. *Inorg. Chim. Acta* **2005**, *358*, 1882. (b) Xiao, H.-P.; Zhu, L.-G. *Inorg. Chem. Commun.* **2006**, *9*, 1125.

(15) (a) Sun, Y.-Q.; Zhang, J.; Yang, G.-Y. *Chem. Commun.* **2006**, 1947. (b) Peng, M.-X.; Hong, C.-G.; Tan, C.-K.; Chen, J.-C.; Tong, M.-L. *J. Chem. Crystallogr.* **2006**, *36*, 703.

(16) (a) Tang, S.-F.; Song, J.-L.; Mao, J.-G. *Eur. J. Inorg. Chem.* **2006**, 2011. (b) Zhou, X.-P.; Li, D.; Wu, T.; Zhang, X. *Dalton Trans.* **2006**, 2435.

(17) (a) Han, L.; Bu, X.; Zhang, Q.; Feng, P. *Inorg. Chem.* **2006**, *45*, 5736. (b) Wang, Y.-T.; Fan, H.-H.; Wang, H.-Z.; Chen, X.-M. *Inorg. Chem.* **2005**, *44*, 4148.

(18) (a) Li, X.; Cao, R.; Guo, Z.; Wang, Y.; Zhu, X. *J. Mol. Struct.* **2006**, *798*, 64. (b) Zhang, J.-P.; Lin, Y.-Y.; Huang, X.-C.; Chen, X.-M. *Cryst. Growth Des.* **2006**, *6*, 519.

(19) *SAINT data collection and procedure software for the SMART system*; Siemens Analytical X-ray Instruments, Inc.: Madison, WI, 1995.

(20) *SHELXTL*, version 5.0; Siemens Analytical X-ray Instruments Inc.: Madison, WI, 1995.

(21) *Software for the SMART System V5.04 and SHELXTL V 5.1*; Bruker-Siemens Analytical X-ray Instrument, Inc.: Madison, WI, 1998.

(22) Rodriguez-Carvajal, J. *Physica B* **1993**, *192*, 5.

(23) Dong, G.-Y.; Cui, G.-H.; Lin, J. *Acta Crystallogr., Sect. E* **2006**, *E62*, 738.

(24) Zhou, Y.-F.; Jiang, F.-L.; Yuan, D.-Q.; Wu, B.-L.; Hong, M.-C. *J. Mol. Struct.* **2005**, *743*, 21.

(25) Cui, G.-H.; Li, J.-R.; Zhang, R.-H.; Bu, X.-H. *J. Mol. Struct.* **2005**, *740*, 187.

(26) He, Q.; Zi, J.-F.; Zhang, F.-J. *Acta Crystallogr., Sect. E* **2006**, *E62*, 1266.

(27) Seguatni, A.; Fakhfakh, M.; Vauley, M. J.; Jouini, N. *J. Solid State Chem.* **2004**, *177* (10), 3402.

(28) Spek, A. L. *Acta Crystallogr. A* **1990**, *46*, C34.

(29) Tanaka, D.; Kitagawa, S. *Chem. Mater.* **2008**, *20*, 922.

(30) De Lill, D. T.; Cahill, C. *Cryst. Growth Des.* **2007**, *7* (12), 2390.

(31) (a) Wells, A. F. *Structural Inorganic Chemistry*, 5th ed.; Oxford University Press: Oxford, 1984. (b) Wells, A. F. *3-D Nets and Polyhedra*; Wiley: New York, 1977. (c) Wells, A. F. *Further Studies of 3-D Nets*; ACA monograph 8, 1979. (d) Smith, J. V. *Chem. Rev.* **1988**, *88*, 149. (e) Smith, J. V. *Tetrahedral Frameworks of Zeolites, Clathrates and Related Materials*; Landolt-Boörnstein New Series IV/14 Subvolume A; Springer: Berlin, 2000. (f) O'Keeffe, M.; Hyde, B. G. *Crystal Structures I: Patterns and Symmetry*; Mineralogical Society of America: Washington, 1996. (g) O'Keeffe, M. *Z. Kristallogr.* **1991**, *196*, 21. (h) O'Keeffe, M.; Philos, B. G.; Hyde, S. T. *Trans. R. Soc., London* **1980**, *295*, 553. (i) O'Keeffe, M.; Hyde, S. T. *Zeolites* **1997**, *19*, 370. (j) Su, C. Y.; Smith, M. D.; Goforth, A. M.; zur Loye, H. C. *Inorg. Chem.* **2004**, *43*, 6881. (k) Su, C. Y.; Cai, Y. P.; Chen, C. L.; Kang, B. S. *Inorg. Chem.* **2001**, *40*, 2210.

(32) Blatov, V. A.; Proserpio, D. M. *Acta Crystallogr.* **2009**, *A65*, 202.

(33) (a) Blatov, V. A. *IUCr Comp. Comm. Newslett.* **2006**, *7*, 4. (b) Blatov, V. A.; Carlucci, L.; Ciani, G.; Proserpio, D. M. *Cryst. Eng. Comm.* **2004**, *6*, 377.

(34) Eddaoudi, M.; Moler, D.; Li, H.; Chen, B.; Reineke, T. M.; O'Keeffe, M.; Yaghi, O. M. *Acc. Chem. Res.* **2001**, *34*, 319.

(35) Rosi, N. L.; Kim, J.; Eddaoudi, M.; Chen, B.; O'Keeffe, M.; Yaghi, O. M. *J. Am. Chem. Soc.* **2005**, *127*, 1504.

(36) International Centre for Difraction Data. JPCDS database. PDF-2, 2003.

(37) Bernini, M. C.; Garro, J. C.; Brusau, E. V.; Narda, G. E.; Varetti, E. L. *J. Mol. Struct.* **2008**, *888*, 113.